Contributions to Mineralogy and Petrology (2021) 176:11
https://doi.org/10.1007/s00410-020-01768-z

ORIGINAL PAPER

Experimental recalibration of the Cr-in-clinopyroxene geobarometer: improved precision and reliability above 4.5 GPa

Z. J. Sudholz[1] · G. M. Yaxley[1] · A. L. Jaques[1] · G. P. Brey[2]

Received: 2 September 2020 / Accepted: 22 December 2020 / Published online: 28 January 2021

Abstract

The pressure dependence of the exchange of Cr between clinopyroxene and garnet in peridotite is applicable as a geobarometer for mantle-derived Cr-diopside xenocrysts and xenoliths. The most widely used calibration (Nimis and Taylor Contrib Miner Petrol 139: 541–554, 2000; herein NT00) performs well at pressures below 4.5 GPa, but has been shown to consistently underestimate pressures above 4.5 GPa. We have experimentally re-examined this exchange reaction over an extended pressure, temperature, and compositional range using multi-anvil, belt, and piston cylinder apparatuses. Twenty-nine experiments were completed between 3–7 GPa, and 1100–1400 °C in a variety of compositionally complex lherzolitic systems. These experiments are used in conjunction with several published experimental datasets to present a modified calibration of the widely-used NT00 Cr-in-clinopyroxene (Cr-in-cpx) single crystal geobarometer. Our updated calibration calculates P (GPa) as a function of T (K), CaCr Tschermak activity in clinopyroxene $\left(a^{\text{cpx}}_{\text{CaCrTs}}\right)$, and Cr/(Cr + Al) (Cr#) in clinopyroxene. Rearranging experimental results into a $2n$ polynomial using multiple linear regression found the following expression for pressure:

$$P(\text{GPa}) = 11.03 + \left(-T(\text{K})\ \ln(a^{\text{cpx}}_{\text{CaCrTs}}) \times 0.001088\right) + \left(1.526 \times \ln\left(\frac{\text{Cr\#}^{\text{cpx}}}{T(\text{K})}\right)\right)$$

where $\text{Cr\#}^{\text{cpx}} = \left(\frac{\text{Cr}}{\text{Cr+Al}}\right)$, $a^{\text{cpx}}_{\text{CaCrTs}} = \text{Cr} - 0.81 \cdot \text{Cr\#}^{\text{cpx}} \cdot (\text{Na} + \text{K})$, with all mineral components calculated assuming six oxygen anions per formula unit in clinopyroxene.

Temperature (K) may be calculated through a variety of geothermometers, however, we recommend the NT00 single crystal, enstatite-in-clinopyroxene (en-in-cpx) geothermometer. The pressure uncertainty of our updated calibration has been propagated by incorporating all analytical and experimental uncertainties. We have found that pressure estimates below 4 GPa, between 4–6 GPa and above 6 GPa have associated uncertainties of 0.31, 0.35, and 0.41 GPa, respectively. Pressures calculated using our calibration of the Cr-in-cpx geobarometer are in good agreement between 2–7 GPa, and 900–1400 °C with those estimated from widely-used two-phase geobarometers based on the solubility of alumina in orthopyroxene coexisting with garnet. Application of our updated calibration to suites of well-equilibrated garnet lherzolite and garnet pyroxenite xenoliths and xenocrysts from the Diavik-Ekati kimberlite and the Argyle lamproite pipes confirm the accuracy and precision of our modified geobarometer, and show that PT estimates using our revised geobarometer result in systematically steeper paleogeotherms and higher estimates of the lithosphere−asthenosphere boundary compared with the original NT00 calibration.

Keywords Geothermobarometry · Lherzolite · Mantle · Diopside · Chromium · Diamonds · Lithospheric mantle · Single crystal geothermobarometry · Cratonic lithosphere · Kimberlites · Xenolith · Peridotite · Experimental petrology · Multi anvil · Piston cylinder

Introduction

Experimental studies on garnet lherzolites have demonstrated that the solubility of Cr in clinopyroxene (cpx) is pressure (P) dependent (Brey et al. 1990). This relationship has previously been used empirically to calibrate the NT00

Communicated by Daniela Rubatto.

✉ Z. J. Sudholz
Zachary.sudholz@anu.edu.au

Extended author information available on the last page of the article

Cr-in-cpx geobarometer for chrome-rich (> 0.50 wt% Cr_2O_3) cpx derived from garnet lherzolites. Their geobarometer was calibrated using previously published data (Nickel 1986; Brey et al. 1990; Taylor 1998) obtained from experimental studies on a variety of synthetic fertile to refractory lherzolite starting compositions over a pressure–temperature (PT) range of 2–6 GPa and 900–1400 °C. The majority of the experiments used in the NT00 calibration were conducted at $P < 4$ GPa. The application of this geobarometer to natural and experimental datasets has confirmed its reliability from 2 to 4 GPa. As a result, the NT00 geothermobarometer has proved to be an important petrological tool for defining PT conditions and mantle lithospheric geotherms, essential for understanding both the thermotectonic and chemical evolution of the sub-continental lithosphere (Mather et al. 2011) and in assessing the diamond-bearing potential of kimberlites (Grütter et al. 2004; Cookenboo and Grütter 2010) in situations for which traditional two-phase geothermobarometry has not been feasible. To accurately study the lithosphere from which garnet lherzolites are sampled, which ranges in thickness up to 300 km (Gung et al. 2003; Lee et al. 2005), reliable P estimates above 4 GPa are critical. Application of the NT00 geobarometer to experimental and natural samples derived from $P > 4$ GPa suggest that it progressively and systematically underestimates P by as much as 1 GPa (Shirey et al. 2013; Ziberna et al. 2016). Despite this, the NT00 geobarometer has remained widely used and is currently the only available major element single crystal geobarometer for garnet lherzolites. A recent empirical correction of the Cr-in-cpx geobarometer was proposed by Nimis et al. (2020) as an interim measure by recalibrating the original NT00 geobarometer against pressures determined by the Al-in-orthopyroxene geobarometer of Nickel and Green (1985) with the modification by Carswell (1991). Although this correction results in an overall improved agreement with Al-in-orthopyroxene P estimates, it has larger uncertainties, especially at high P (> 4.5 GPa).

In the following study, the solubility of Cr in lherzolitic cpx is re-examined using experimental methods. We present data from twenty-nine new experiments conducted at 3–7 GPa and 1100–1400 °C, which form the basis of a high-P experimental database. This database is used in conjunction with similar experiments from Brey et al. (1990), Taylor (1998), and Walter (1998) to establish an updated Cr-in-cpx geobarometer more suitable for higher mantle pressures. The reliability of our updated calibration is rigorously tested on previously published well-equilibrated natural garnet lherzolite and garnet pyroxenite xenolith datasets from the Diavik-Ekati kimberlite pipes, with P estimates compared to the results obtained from various internally consistent two-phase geothermobarometers.

Methods

Experimental methods

We used three synthetic lherzolite compositions which are variants of the MORB-pyrolite composition of Green and Falloon (1998) (Table 1), recalculated to contain 40% less olivine. The MORB-pyrolite (MPY-40) starting composition is an estimate of the composition of the fertile upper mantle (Green, 2015) and formed the basis for all experimental compositions used in this study. A Cr-enriched MPY-40 composition (Cr-MPY-40) was used in several experiments between 3–4 GPa and 1200–1300 °C. This composition was used to broaden the range of the $\ln\left(\frac{Cr\#^{cpx}}{T(K)}\right)$ term (see below) in our calibration, and to synthesise garnet and cpx with Cr# values $\left(Cr\# = \left(\frac{Cr}{Cr+Al}\right)\right)$, similar to those found in depleted cratonic lherzolites ($Cr\#^{cpx}$ 0.25–0.30). A Hawaiian pyrolite (Green 2015) (HPY-40) starting composition was used in several experimental runs to test the precision and accuracy of our geobarometer on a non MPY-40 starting composition.

Starting mixtures were prepared by blending oxide and carbonate powders and synthetic fayalite under acetone, using well-established techniques (Yaxley and Green, 1998). The starting mixtures were loaded into graphite crucibles enclosed with a graphite lid. The graphite capsule was contained in 2.3 × 3.5 mm outside diameter platinum (Pt) capsule which was triple crimped on each end, welded shut, and housed in 12.5 mm length MgO tubing. A 1 mm MgO disk was used to separate the Pt capsule from the thermocouple. Half-inch diameter NaCl sleeves were used as the pressure medium for all piston cylinder experiments. A 12.5 mm length cylindrical graphite furnace was placed between the MgO tubing and the outer NaCl pressure medium. For

Table 1 Composition of starting mixtures used in experiments for the calibration of the Cr-in-cpx geobarometer

Oxide (wt%)	Cr-MPY-40	MPY-40	HPY-40
SiO_2	46.48	47.15	47.90
TiO_2	0.28	0.28	1.18
Al_2O_3	7.18	7.28	5.91
FeO	7.17	7.27	8.81
MnO	0.12	0.12	0.13
MgO	30.13	30.57	28.80
CaO	5.55	5.63	5.14
Na_2O	0.65	0.66	0.95
Cr_2O_3	2.17	0.75	0.72
NiO	0.29	0.29	0.13
Total	100	100	100
Mg#	0.88	0.88	0.85

experiments near and above the NaCl solidus, a Pyrex glass tube was positioned between the NaCl pressure medium and the graphite furnace to prevent the melting of the NaCl.

All experiments were completed at the Research School of Earth Sciences, Australian National University. Experiments at 3, 3.5 and 4 GPa were performed on a 150-tonne end-loaded piston cylinder apparatus from 1100 to 1400 °C. Temperature was measured by a type B Pt–Rh thermocouple. The run durations of these experiments were typically > 120 h. For experiments at 5 and 6 GPa a modified ultra-high pressure, 500-tonne end-loaded piston cylinder was used. The *T* of these experiments ranged from 1100 to 1400 °C and was also measured with a type B Pt–Rh thermocouple. The run times of these experiments varied from 120 to 168 h. Experiments completed on the 500-tonne piston cylinder were typically pressurized over 1 h and then heated over 30 min. Experimental PT conditions for both piston cylinders were calibrated by the quartz–coesite transition (Bose and Ganguly 1995). A 1200-tonne, Kawai-style split sphere 6/8 multi-anvil apparatus was used for experiments conducted at 7 GPa. The same starting compositions and capsule materials were used as described above. All multi-anvil experiments used a 14/8 anvil cell configuration, and a G2 COMPRESS assembly. Further details of this assembly can be found in Leinenweber et al. (2012). Multi-anvil experiments were pressurized over a 24-h period and heated over 1 h. The *T* of the multi-anvil experiments was measured with a W–Re thermocouple. The run duration of multi-anvil experiments ranged between 6 and 48 h. The run conditions (*P*, *T*, starting composition, duration) of experiments completed in this study are listed in Table 2. The run conditions of the previously published experiments used in our calibration are listed in Table 3. These published experimental datasets are described in greater detail below.

In preparation for imaging and quantitative analyses, all capsules were removed from their assemblies and mounted in epoxy resin. Once set, capsule mounts were polished down to expose the experimental charge (starting material) and re-impregnated with epoxy under vacuum to seal any cracks. The capsule mounts were polished down to a ¼ µm grit using a diamond lapse and coated with a thin film of carbon for electron probe microanalysis.

Table 2 Summary of run conditions of the experiments used in this study

Source	Experimental no.	*P* (GPa)	*T* (°C)	Duration (h)	Starting composition
This study	PT.22 R	3	1150	120	MPY-40
This study	PT.1	3	1200	120	MPY-40
This study	HPT.3	3	1200	120	HPY-40
This study	CRPT.16	3	1250	120	Cr-MPY-40
This study	PT.29 R	3.5	1150	120	MPY-40
This study	HPT.4	3.5	1200	120	HPY-40
This study	CRPT.22 R	3.5	1200	120	Cr-MPY-40
This study	CRPT.21	3.5	1250	120	Cr-MPY-40
This study	PT.37	3.5	1300	72	MPY-40
This study	PT.47	3.5	1350	72	MPY-40
This study	PT.35B R	3.5	1350	72	MPY-40
This study	HPT.6	3.5	1400	72	HPY-40
This study	PT.50	3.5	1400	72	MPY-40
This study	PT.6	4	1100	120	MPY-40
This study	PT.2	4	1200	120	MPY-40
This study	CRPT.1	4	1200	120	Cr-MPY-40
This study	CRPT.3 R	4	1200	120	Cr-MPY-40
This study	PT.59	4	1300	72	MPY-40
This study	PT.5	4	1300	120	MPY-40
This study	PT.46	4	1350	72	MPY-40
This study	CRPT.3	4	1350	72	Cr-MPY-40
This study	PT.8	4	1400	72	MPY-40
This study	PT.49	4	1400	72	MPY-40
This study	PT.12	5	1200	168	MPY-40
This study	PT.60	5	1250	72	MPY-40
This study	PT.40 R	5	1300	72	MPY-40
This study	PT.45	5	1400	72	MPY-40
This study	PT.14	6	1200	168	MPY-40

Table 3 Summary of run conditions of previously published experiments used in our calibration

Source	Experimental no.	*P* (GPa)	*T* (°C)	Starting composition
Walter (1998)	5001	5	1680	Pyrolite
Walter (1998)	6002	6	1670	Pyrolite
Walter (1998)	6004	6	1700	Pyrolite
Walter (1998)	6001	6	1710	Pyrolite
Walter (1998)	6007	6	1740	Pyrolite
Walter (1998)	6005	6	1755	Pyrolite
Walter (1998)	7001	7	1740	Pyrolite
Walter (1998)	7007	7	1790	Pyrolite
Walter (1998)	7002	7	1810	Pyrolite
Walter (1998)	7005	7	1820	Pyrolite
Taylor (1998)	T2103	2	1100	HPY-40
Taylor (1998)	T2163	2	1150	HPY-40
Taylor (1998)	T2188	2	1175	HPY-40
Taylor (1998)	T2234	2	1200	HPY-40
Taylor (1998)	T2591	2.2	1100	HPY-40
Taylor (1998)	T2258	2.25	1190	HPY-40
Taylor (1998)	T2256	2.25	1230	HPY-40
Taylor (1998)	T2308	2.5	1050	HPY-40
Taylor (1998)	T1904	2.5	1100	HPY-40
Taylor (1998)	T1926	2.5	1150	HPY-40
Taylor (1998)	T2232	2.5	1250	HPY-40
Brey et al. (1990)	347 SCS + SC-1	5	900	Natural
Brey et al. (1990)	462 JA + NAT1/CA	5	1000	Natural
Brey et al. (1990)	249	5	1100	Natural
Brey et al. (1990)	320 SCS + SC-1	5	1200	Natural
Brey et al. (1990)	407	5	1300	Natural
Brey et al. (1990)	248	5	1400	Natural
Brey et al. (1990)	418	6	1300	Natural
Brey et al. (1990)	419	6	1400	Natural

See Taylor (1998), Walter (1998), and Brey et al. (1990) for details of starting compositions and run durations

Analytical methods

Quantitative analyses of the experimental run products were done by wavelength dispersive spectroscopy (WDS) on a JEOL JXA-8530F + electron probe micro analyser (EPMA) at the Centre for Advanced Microscopy (CAM), Australian National University. A 15 kV accelerating voltage, a beam current of 10 nA, and 1 µm spot size were used routinely for most mineral analyses. Counting times were 20 s (peak and background) for major elements and 30–40 s for minor elements with a total analytical time of approximately 2–3 min. The calibrations were made using a mix of synthetic and natural *ASTIMEX Mineralogy* standards as follows: Na (albite), Mg (periclase and olivine), Al (sanidine and pyrope), Si (sanidine and diopside), Ca (diopside), Ti (rutile), Cr (chromite), Mn (rhodonite), Fe (haematite and magnetite), and Ni (pentlandite). The limits of detection were typically 70–180 ppm, equivalent to 0.01–0.03 wt% oxide. The data correction was done using the 'PAP model' (Pouchou and Pichoir 1991). A total of 10–20 EPMA analyses were typically performed on cpx grains within each sample. Fewer analyses were performed for runs with low modal abundances of cpx. The number of analyses on garnet (grt), orthopyroxene (opx) and olivine (ol) grains typically ranged between 5 and 15 for each sample. Only cpx that crystallised in experiments containing garnet lherzolite or garnet pyroxenite assemblages were used in our calibration. The quality of major and minor element data for cpx was filtered following the strict protocols of Ziberna et al. (2016) whereby cpx analyses with totals < 98 and > 102 wt%, and cation totals < 3.98 and > 4.02 (calculated on the basis of six oxygens in clinopyroxene) were rejected. Published cpx analyses from the Walter (1998) and Taylor (1998) experimental datasets also adhere to the data quality protocols of Ziberna et al. (2016). Because the Brey et al. (1990) analyses were normalized to 100 wt% and four cations in clinopyroxene, it is not possible to apply these data quality protocols to their experiments. However, given that these experiments were used to calibrate the widely-used Brey and Köhler (1990) set of geothermobarometers, it is reasonable to conclude that they are of sufficient quality to be incorporated into the experimental dataset used in this study. The averages of the accepted mineral analyses (in oxide wt%) for each experiment completed in this study are listed in Table 4.

Results

Our experiments were generally successful at synthesising a garnet lherzolite, and/or garnet pyroxenite equilibrium assemblage. The size of crystals produced from our experiments typically varied from 10 to 40 µm (Fig. 1a). Garnet and orthopyroxene were usually the largest of these phases (> 25 µm). Back-scattered electron (BSE) images were used to qualitatively identify inhomogeneous regions within crystals prior to WDS analysis. Well equilibrated runs contained phases with well-defined grain boundaries (Fig. 1a) and cation abundances that were approximately homogenous across the entire experimental charge. The presence of significant Fe^{3+} in garnet and clinopyroxene is unlikely given that our experiments equilibrated in reducing conditions (controlled by the graphite furnace at around the CCO buffer) not suitable for appreciable Fe^{2+} oxidation. Further, the lack of large deviations on the X^{2+} and X^{3+} sites of garnet and clinopyroxene (Table 4) are inconsistent with the presence of large quantities of Fe^{3+}.

Table 4 Major element analyses by WDS EPMA data for the experimental run products

Experiment no.		Pressure	Temperature	Duration	*n*	SiO_2	TiO_2	Al_2O_3	Cr_2O_3	FeO total	MnO	MgO	NiO	CaO	Na_2O	Total
Grt	PT.22 R	3	1150	120	5	41.53	0.36	22.21	1.84	6.32	0.22	20.45	0.03	6.05	0.06	99.07
Grt	PT.1	3	1200	120	6	42.38	0.27	23.27	1.58	6.77	0.21	20.49	0.02	5.77	0.04	100.79
Grt	HPT.3	3	1200	120	12	41.90	0.03	22.09	1.64	9.26	0.27	19.68	0.01	5.04	0.02	99.94
Grt	CRPT.16	3	1250	120	11	41.59	0.35	20.85	3.15	7.65	0.22	19.28	0.06	6.50	0.03	99.70
Grt	PT.29 R	3.5	1150	120	3	41.60	0.26	21.84	1.55	10.33	0.21	18.58	0.05	5.57	0.08	100.07
Grt	HPT.4	3.5	1200	120	7	42.29	0.02	22.24	1.76	10.24	0.28	19.36	0.01	4.89	0.06	101.14
Grt	CRPT.22 R	3.5	1200	120	11	41.20	0.48	19.23	4.37	7.74	0.23	19.17	0.07	6.25	0.05	98.80
Grt	CRPT.21	3.5	1250	120	17	41.50	0.38	20.73	3.60	7.21	0.21	19.43	0.03	6.26	0.02	99.36
Grt	PT.37	3.5	1300	120	11	41.97	0.37	21.84	1.79	6.77	0.20	20.69	0.03	5.65	0.04	99.34
Grt	PT.47	3.5	1350	120	19	42.43	0.23	21.92	2.09	5.21	0.19	21.62	0.02	6.07	0.03	99.80
Grt	PT.35B R	3.5	1350	120		42.36	0.26	21.71	2.10	6.05	0.17	20.56	0.01	5.91	0.05	99.18
Grt	HPT.6	3.5	1400	120	10	41.62	0.02	22.51	1.93	7.76	0.23	21.15	0.01	4.77	0.03	100.05
Grt	PT.50	3.5	1400	120	12	41.98	0.29	22.03	2.28	5.71	0.18	21.82	0.01	5.79	0.03	100.12
Grt	PT.6	4	1100	120	6	42.26	0.29	23.10	1.23	6.48	0.20	20.56	0.03	5.82	0.02	99.99
Grt	PT.2	4	1200	120	10	42.50	0.28	23.00	1.71	6.93	0.19	20.66	0.02	5.41	0.05	100.77
Grt	CRPT.1	4	1200	120	14	41.47	0.54	19.52	5.21	6.55	0.24	20.32	0.02	6.16	0.05	100.08
Grt	CRPT.3 R	4	1200	120	14	41.74	0.59	19.45	4.15	7.95	0.24	18.90	0.06	6.57	0.05	99.71
Grt	PT.5	4	1300	120	6	42.55	0.14	21.90	2.91	4.75	0.16	22.40	0.01	4.91	0.02	99.74
Grt	PT.59	4	1300	120	11	41.85	0.43	22.33	1.75	6.33	0.19	21.63	0.05	5.87	0.06	100.50
Grt	PT.46	4	1350	120	17	42.37	0.28	22.38	1.97	5.78	0.17	21.86	0.01	5.57	0.03	100.41
Grt	CRPT.3	4	1350	120	10	41.52	0.52	19.52	5.18	6.18	0.18	20.51	0.02	5.85	0.05	99.53
Grt	PT.8	4	1400	120	7	41.82	0.34	22.20	2.06	6.76	0.19	20.99	0.02	5.37	0.03	99.77
Grt	PT.49	4	1400	120	18	42.67	0.20	22.31	2.25	4.82	0.16	22.09	0.01	5.67	0.03	100.20
Grt	PT.12	5	1200	168	9	42.60	0.32	22.78	1.68	5.08	0.19	22.33	0.02	5.05	0.04	100.08
Grt	PT.60	5	1250	120	11	41.65	0.31	22.63	1.68	6.88	0.18	20.85	0.02	5.34	0.04	99.57
Grt	PT.40 R	5	1300	120	10	41.62	0.24	21.94	1.88	7.43	0.17	20.77	0.04	5.09	0.03	99.21
Grt	PT.45	5	1400	168	10	42.58	0.24	22.67	1.68	6.17	0.17	21.57	0.03	4.77	0.03	99.91
Grt	PT.14	6	1200	168	9	41.94	0.36	22.78	1.51	5.80	0.18	21.82	0.02	4.95	0.04	99.39
Grt	PT.27	7	1200	12	14	42.38	0.44	22.02	1.38	7.25	0.19	21.49	0.11	4.34	0.09	99.68

Experiment no.	Si	Ti	Al	Fe^{2+}	Mn	Mg	Ca	Na	Cr	Ni	Total
PT.22 R	2.974	0.019	1.875	0.378	0.013	2.183	0.464	0.009	0.104	0.002	8.021
PT.1	2.977	0.014	1.927	0.398	0.012	2.146	0.434	0.005	0.088	0.001	8.004
HPT.3	3.001	0.002	1.864	0.554	0.016	2.101	0.386	0.003	0.093	bdl	8.021
CRPT.16	2.994	0.019	1.769	0.461	0.014	2.069	0.502	0.004	0.180	0.004	8.014
PT.29 R	2.996	0.014	1.854	0.622	0.013	1.995	0.430	0.011	0.088	0.003	8.025

Table 4 (continued)

Experiment no.	Si	Ti	Al	Fe^{2+}	Mn	Mg	Ca	Na	Cr	Ni	Total
HPT.4	3.003	0.001	1.861	0.608	0.017	2.049	0.372	0.008	0.099	0.001	8.020
CRPT.22 R	3.008	0.026	1.654	0.473	0.014	2.086	0.489	0.008	0.253	0.004	8.016
CRPT.21	2.993	0.021	1.761	0.435	0.013	2.089	0.484	0.003	0.205	0.001	8.005
PT.37	2.998	0.020	1.838	0.404	0.012	2.203	0.433	0.005	0.101	0.002	8.015
PT.47	3.000	0.012	1.826	0.308	0.011	2.279	0.460	0.005	0.117	0.001	8.019
PT.35B R	3.022	0.014	1.825	0.361	0.010	2.187	0.452	0.006	0.119	0.001	7.996
HPT.6	2.960	0.001	1.887	0.462	0.014	2.243	0.363	0.004	0.109	0.001	8.043
PT.50	2.968	0.015	1.835	0.338	0.011	2.300	0.438	0.004	0.128	0.001	8.037
PT.6	2.987	0.015	1.924	0.383	0.012	2.166	0.441	0.003	0.069	0.002	8.002
PT.2	2.987	0.015	1.905	0.407	0.011	2.165	0.407	0.006	0.095	0.001	8.001
CRPT.1	2.978	0.029	1.652	0.393	0.015	2.175	0.474	0.007	0.296	0.001	8.022
CRPT.3 R	3.020	0.032	1.659	0.481	0.015	2.038	0.509	0.008	0.237	0.004	8.003
PT.5	2.999	0.007	1.819	0.280	0.010	2.353	0.371	0.003	0.162	bdl	8.004
PT.59	2.954	0.023	1.858	0.374	0.012	2.276	0.444	0.008	0.098	0.003	8.049
PT.46	2.980	0.015	1.855	0.340	0.010	2.292	0.420	0.004	0.109	0.001	8.025
CRPT.3	2.989	0.028	1.656	0.372	0.011	2.201	0.451	0.007	0.295	0.001	8.011
PT.8	2.970	0.016	1.873	0.419	0.010	2.217	0.405	0.004	0.112	bdl	8.022
PT.49	2.996	0.011	1.846	0.283	0.010	2.311	0.426	0.004	0.125	bdl	8.011
PT.12	2.988	0.017	1.883	0.298	0.011	2.335	0.380	0.005	0.093	0.001	8.010
PT.60	2.966	0.017	1.899	0.410	0.011	2.213	0.408	0.006	0.094	0.001	8.024
PT.40 R	2.983	0.013	1.852	0.445	0.010	2.219	0.391	0.005	0.106	0.002	8.027
PT.45	3.002	0.013	1.883	0.364	0.010	2.267	0.360	0.004	0.094	0.002	7.998
PT.14	2.972	0.019	1.902	0.344	0.011	2.305	0.376	0.005	0.085	0.001	8.019
PT.27	3.008	0.024	1.842	0.430	0.011	2.274	0.330	0.012	0.078	0.006	8.014

Experiment no.		Pressure	Temperature	Duration	*n*	SiO_2	TiO_2	Al_2O_3	Cr_2O_3	FeO total	MnO	MgO	NiO	CaO	Na_2O	Total
Olv	PT.22 R	3	1150	120	6	40.85	0.01	0.15	0.09	9.78	0.07	49.24	0.05	0.14	0.05	100.44
Olv	PT.1	3	1200	120	6	40.68	0.02	0.07	0.09	9.84	0.10	49.55	0.04	0.15	0.04	100.56
Olv	HPT.3	3	1200	120	20	39.57	bdl	0.05	0.08	14.36	0.13	45.54	0.12	0.16	0.03	100.05
Olv	CRPT.16	3	1250	120	7	40.45	0.01	0.31	0.34	5.19	0.07	53.18	0.47	0.21	0.04	100.27
Olv	PT.29 R	3.5	1150	120	8	40.93	0.02	0.28	0.07	8.38	0.07	49.66	0.99	0.33	0.06	100.79
Olv	HPT.4	3.5	1200	120	12	39.01	bdl	0.04	0.08	14.87	0.14	46.00	0.08	0.15	0.02	100.40
Olv	CRPT.22 R	3.5	1200	120	12	39.60	0.03	0.12	0.32	10.02	0.08	47.07	1.36	0.21	0.04	98.83
Olv	CRPT.21	3.5	1250	120	11	40.22	0.01	0.14	0.21	10.45	0.08	48.35	0.29	0.18	0.02	99.95
Olv	PT.37	3.5	1300	120	7	40.05	0.01	0.10	0.08	9.74	0.10	48.34	0.52	0.26	0.04	99.24
Olv	PT.47	3.5	1350	120	12	40.53	0.01	0.14	0.12	7.07	0.10	49.96	0.16	0.24	0.02	98.35

Table 4 (continued)

Experiment no.		Pressure	Temperature	Duration	*n*	SiO_2	TiO_2	Al_2O_3	Cr_2O_3	FeO total	MnO	MgO	NiO	CaO	Na_2O	Total
Olv	PT.35B R	3.5	1350	120	6	40.65	0.01	0.14	0.11	8.84	0.10	49.60	0.03	0.23	0.03	99.74
Olv	HPT.6	3.5	1400	120	12	38.70	Bdl	0.15	0.11	13.20	0.13	47.81	0.01	0.25	0.03	100.39
Olv	PT.50	3.5	1400	120	6	39.87	0.01	0.13	0.13	8.62	0.10	49.49	0.07	0.25	0.04	98.70
Olv	PT.6	4	1100	120	8	40.42	0.02	0.10	0.06	7.86	0.08	49.91	0.77	0.14	0.01	99.36
Olv	PT.2	4	1200	120	9	40.54	0.01	0.06	0.07	9.99	0.09	49.11	0.16	0.12	0.06	100.22
Olv	CRPT.1	4	1200	120	14	40.21	0.02	0.10	0.21	8.56	0.09	49.88	0.33	0.22	0.04	99.67
Olv	CRPT.3 R	4	1200	120	4	40.30	0.03	0.18	0.41	10.09	0.08	47.96	0.63	0.21	0.04	99.93
Olv	PT.5	4	1300	120	2	41.43	0.01	0.12	0.10	7.38	0.06	48.98	0.01	0.17	0.03	98.29
Olv	PT.59	4	1300	120	8	41.24	0.01	0.14	0.10	9.01	0.09	49.72	0.79	0.36	0.05	101.52
Olv	PT.46	4	1350	120	14	40.32	0.01	0.13	0.11	8.58	0.09	49.57	0.07	0.27	0.04	99.19
Olv	CRPT.3	4	1350	120	11	40.93	0.02	0.14	0.24	8.66	0.08	49.44	0.43	0.21	0.04	100.19
Olv	PT.8	4	1400	120	6	40.27	bdl	0.11	0.12	10.37	0.10	48.57	0.28	0.23	0.03	100.08
Olv	PT.49	4	1400	120	13	41.31	0.01	0.13	0.09	5.91	0.08	51.50	0.02	0.27	0.03	99.35
Olv	PT.12	5	1200	168	12	41.74	0.02	0.09	0.06	5.60	0.07	52.50	0.55	0.12	0.01	100.76
Olv	PT.60	5	1250	120	11	39.79	0.01	0.06	0.07	9.28	0.06	48.85	0.30	0.18	0.02	98.62
Olv	PT.40 R	5	1300	120	5	39.38	0.01	0.07	0.08	10.11	0.06	49.29	0.47	0.36	0.02	99.86
Olv	PT.45	5	1400	168	10	40.14	0.01	0.09	0.08	10.39	0.09	49.71	0.25	0.22	0.03	101.01
Olv	PT.14	6	1200	168	5	40.62	0.01	0.05	0.05	6.52	0.06	52.02	0.23	0.12	0.02	99.69
Olv	PT.27	7	1200	12	7	40.49	0.03	0.24	0.07	7.81	0.08	49.15	1.23	0.30	0.04	99.42

Experiment no.	Si	Ti	Al	Fe^{2+}	Mn	Mg	Ca	Na	Cr	Ni	Total
PT.22 R	0.996	bdl	0.004	0.200	0.001	1.791	0.004	0.003	0.002	0.001	3.002
PT.1	0.992	bdl	0.002	0.201	0.002	1.801	0.004	0.002	0.002	0.001	3.007
HPT.3	0.991	bdl	0.002	0.301	0.003	1.701	0.004	0.001	0.002	0.002	3.007
CRPT.16	0.974	bdl	0.009	0.105	0.001	1.908	0.005	0.002	0.006	0.009	3.019
PT.29 R	0.994	bdl	0.008	0.170	0.001	1.797	0.009	0.003	0.001	0.019	3.003
HPT.4	0.978	bdl	0.001	0.312	0.003	1.719	0.004	0.001	0.002	0.002	3.021
CRPT.22 R	0.991	0.001	0.004	0.210	0.002	1.757	0.006	0.002	0.006	0.027	3.004
CRPT.21	0.991	bdl	0.004	0.215	0.002	1.777	0.005	0.001	0.004	0.006	3.005
PT.37	0.992	bdl	0.003	0.202	0.002	1.786	0.007	0.002	0.002	0.010	3.006
PT.47	0.999	bdl	0.004	0.146	0.002	1.835	0.006	0.001	0.002	0.003	2.999
PT.35B R	0.995	bdl	0.004	0.181	0.002	1.810	0.006	0.001	0.002	0.001	3.002
HPT.6	0.964	bdl	0.004	0.275	0.003	1.776	0.007	0.002	0.002	bdl	3.033
PT.50	0.987	bdl	0.004	0.178	0.002	1.827	0.007	0.002	0.003	0.001	3.011
PT.6	0.992	bdl	0.003	0.161	0.002	1.827	0.004	bdl	0.001	0.015	3.005
PT.2	0.993	bdl	0.002	0.205	0.002	1.794	0.003	0.003	0.001	0.003	3.006

Table 4 (continued)

Experiment no.	Si	Ti	Al	Fe^{2+}	Mn	Mg	Ca	Na	Cr	Ni	Total
CRPT.1	0.986	bdl	0.003	0.178	0.002	1.824	0.006	0.002	0.004	0.007	3.011
CRPT.3 R	0.994	0.001	0.005	0.208	0.002	1.763	0.006	0.002	0.008	0.013	3.000
PT.5	1.019	bdl	0.003	0.152	0.001	1.796	0.005	0.001	0.002	bdl	2.979
PT.59	0.996	bdl	0.004	0.182	0.002	1.790	0.009	0.003	0.002	0.015	3.002
PT.46	0.992	bdl	0.004	0.177	0.002	1.818	0.007	0.002	0.002	0.001	3.006
CRPT.3	0.998	bdl	0.004	0.176	0.002	1.797	0.005	0.002	0.005	0.009	2.998
PT.8	0.991	bdl	0.003	0.213	0.002	1.782	0.006	0.001	0.002	0.006	3.007
PT.49	1.001	bdl	0.004	0.120	0.002	1.860	0.007	0.001	0.002	bdl	2.997
PT.12	0.998	bdl	0.002	0.112	0.001	1.871	0.003	0.001	0.001	0.011	3.000
PT.60	0.989	bdl	0.002	0.193	0.001	1.811	0.005	0.001	0.001	0.006	3.009
PT.40 R	0.974	bdl	0.002	0.209	0.001	1.817	0.010	0.001	0.001	0.009	3.025
PT.45	0.980	bdl	0.003	0.212	0.002	1.809	0.006	0.001	0.002	0.005	3.019
PT.14	0.986	bdl	0.001	0.132	0.001	1.882	0.003	0.001	0.001	0.004	3.013
PT.27	0.995	bdl	0.007	0.160	0.002	1.801	0.008	0.002	0.001	0.024	3.001

Experiment no.		Pressure	Temperature	Duration	*n*	SiO_2	TiO_2	Al_2O_3	Cr_2O_3	FeO total	MnO	MgO	NiO	CaO	Na_2O	Total
Cpx	PT.22 R	3	1150	120	16	53.33	0.25	4.34	1.05	3.26	0.09	18.40	0.08	17.49	1.21	99.49
Cpx	PT.1	3	1200	120	14	53.35	0.27	6.06	1.08	3.52	0.08	17.78	0.01	14.22	2.55	98.90
Cpx	HPT.3	3	1200	120	15	53.27	0.02	5.04	1.18	5.51	0.13	17.96	0.02	13.81	2.07	99.01
Cpx	CRPT.16	3	1250	120	13	52.38	0.22	5.31	1.79	3.16	0.09	18.05	0.15	16.43	1.35	98.95
Cpx	PT.29 R	3.5	1150	120	10	54.30	0.21	3.01	0.96	3.50	0.08	20.11	0.18	15.93	1.18	99.46
Cpx	HPT.4	3.5	1200	120	17	53.59	0.01	4.47	1.08	5.44	0.11	17.83	0.02	14.59	2.02	99.16
Cpx	CRPT.22 R	3.5	1200	120	14	52.60	0.28	3.56	2.19	3.68	0.09	17.98	0.23	16.20	1.63	98.44
Cpx	CRPT.21	3.5	1250	120	16	53.33	0.14	3.20	1.90	3.85	0.09	18.66	0.09	16.61	1.12	98.98
Cpx	PT.37	3.5	1300	120	18	53.63	0.23	4.63	0.84	4.08	0.11	20.11	0.04	14.18	1.37	99.23
Cpx	PT.47	3.5	1350	120	17	52.63	0.18	5.49	0.96	3.38	0.10	20.26	0.03	14.50	1.01	98.53
Cpx	PT.35B R	3.5	1350	120	15	53.35	0.11	4.14	0.85	3.78	0.09	20.51	0.01	15.41	0.82	99.07
Cpx	HPT.6	3.5	1400	120	16	53.33	0.01	5.29	0.87	6.65	0.15	22.03	0.01	9.71	1.25	99.30
Cpx	PT.50	3.5	1400	120	13	53.14	0.15	4.76	0.87	3.80	0.09	22.07	0.00	13.14	0.95	98.97
Cpx	PT.6	4	1100	120	9	53.86	0.16	2.12	0.70	2.66	0.06	18.47	0.13	19.97	0.92	99.05
Cpx	PT.2	4	1200	120	10	54.22	0.28	5.94	1.03	3.57	0.09	17.51	0.02	12.73	3.32	98.70
Cpx	CRPT.1	4	1200	120	13	53.97	0.22	2.70	1.84	3.81	0.09	18.52	0.18	16.74	1.36	99.42
Cpx	CRPT.3 R	4	1200	120	18	53.89	0.22	2.69	1.84	3.82	0.09	18.57	0.18	16.71	1.36	99.36
Cpx	PT.5	4	1300	120	1	54.13	0.14	3.59	0.39	4.92	0.10	24.79	0.02	11.00	0.72	99.80
Cpx	PT.59	4	1300	120	23	54.79	0.18	3.65	0.84	3.70	0.10	20.59	0.13	15.18	1.17	100.33
Cpx	PT.46	4	1350	120	12	53.76	0.13	4.21	0.78	4.26	0.10	22.14	0.03	13.28	1.03	99.73

Table 4 (continued)

Experiment no.		Pressure	Temperature	Duration	*n*	SiO_2	TiO_2	Al_2O_3	Cr_2O_3	FeO total	MnO	MgO	NiO	CaO	Na_2O	Total
Cpx	CRPT.3	4	1350	120	14	54.21	0.18	3.52	2.09	4.45	0.10	20.66	0.09	13.43	1.31	100.04
Cpx	PT.8	4	1400	120	7	54.44	0.16	4.30	0.77	4.62	0.11	21.56	0.04	13.75	1.24	100.99
Cpx	PT.49	4	1400	120	22	54.48	0.10	4.20	0.60	3.45	0.10	22.89	0.01	13.03	0.95	99.81
Cpx	PT.12	5	1200	168	8	55.72	0.14	2.47	0.77	2.92	0.07	19.30	0.09	18.63	1.29	101.38
Cpx	PT.60	5	1250	120	4	54.18	0.10	2.08	0.66	3.79	0.07	21.34	0.05	15.81	0.83	98.90
Cpx	PT.40 R	5	1300	120	14	55.07	0.10	2.25	0.65	3.99	0.08	20.33	0.15	16.40	1.10	100.13
Cpx	PT.45	5	1400	168	18	54.46	0.11	2.84	0.66	4.43	0.10	21.60	0.06	13.86	1.02	99.12
Cpx	PT.14	6	1200	168	1	54.44	0.11	1.86	0.60	2.48	0.05	19.60	0.04	19.29	1.08	99.55
Cpx	PT.27	7	1200	12	14	54.95	0.13	2.09	0.65	3.30	0.08	19.90	0.28	16.46	1.47	99.33

Experiment no.	Si	Ti	Al	Fe^{2+}	Mn	Mg	Ca	Na	Cr	Ni	Total
PT.22 R	1.926	0.007	0.185	0.099	0.003	0.991	0.677	0.085	0.030	0.002	4.003
PT.1	1.925	0.007	0.257	0.106	0.002	0.956	0.550	0.178	0.031	bdl	4.013
HPT.3	1.935	0.001	0.216	0.167	0.004	0.972	0.537	0.146	0.034	0.001	4.012
CRPT.16	1.902	0.006	0.227	0.096	0.003	0.977	0.639	0.095	0.051	0.005	4.000
PT.29 R	1.954	0.006	0.128	0.105	0.003	1.078	0.615	0.083	0.027	0.005	4.004
HPT.4	1.946	bdl	0.191	0.165	0.003	0.965	0.567	0.143	0.031	0.001	4.013
CRPT.22 R	1.929	0.008	0.154	0.113	0.003	0.983	0.636	0.116	0.064	0.007	4.012
CRPT.21	1.941	0.004	0.137	0.117	0.003	1.013	0.648	0.079	0.055	0.003	3.999
PT.37	1.929	0.006	0.196	0.123	0.003	1.078	0.546	0.096	0.024	0.001	4.003
PT.47	1.902	0.005	0.234	0.102	0.003	1.091	0.562	0.071	0.027	0.001	3.998
PT.35B R	1.924	0.003	0.176	0.114	0.003	1.103	0.595	0.057	0.024	bdl	4.001
HPT.6	1.914	bdl	0.224	0.199	0.004	1.178	0.373	0.087	0.025	bdl	4.006
PT.50	1.908	0.004	0.201	0.114	0.003	1.181	0.505	0.066	0.025	bdl	4.008
PT.6	1.962	0.004	0.091	0.081	0.002	1.003	0.779	0.065	0.020	0.004	4.011
PT.2	1.953	0.008	0.252	0.108	0.003	0.940	0.491	0.232	0.029	0.001	4.015
CRPT.1	1.957	0.006	0.115	0.116	0.003	1.001	0.650	0.096	0.053	0.005	4.001
CRPT.3 R	1.955	0.006	0.115	0.116	0.003	1.005	0.650	0.096	0.053	0.005	4.003
PT.5	1.922	0.004	0.150	0.146	0.003	1.313	0.419	0.049	0.011	0.001	4.018
PT.59	1.949	0.005	0.153	0.110	0.003	1.092	0.579	0.080	0.023	0.004	3.998
PT.46	1.920	0.003	0.177	0.127	0.003	1.179	0.508	0.071	0.022	0.001	4.012
CRPT.3	1.939	0.005	0.148	0.133	0.003	1.102	0.515	0.091	0.059	0.003	3.998
PT.8	1.925	0.004	0.179	0.137	0.003	1.136	0.521	0.085	0.022	0.001	4.013
PT.49	1.932	0.003	0.175	0.102	0.003	1.210	0.495	0.065	0.017	bdl	4.002
PT.12	1.973	0.004	0.103	0.086	0.002	1.019	0.706	0.088	0.021	0.003	4.006
PT.60	1.961	0.003	0.089	0.114	0.002	1.151	0.614	0.058	0.019	0.002	4.012

Table 4 (continued)

Experiment no.	Si	Ti	Al	Fe^{2+}	Mn	Mg	Ca	Na	Cr	Ni	Total
PT.40 R	1.972	0.003	0.095	0.119	0.002	1.086	0.629	0.077	0.018	0.004	4.006
PT.45	1.960	0.003	0.120	0.133	0.003	1.159	0.534	0.071	0.019	0.002	4.003
PT.14	1.966	0.003	0.079	0.075	0.002	1.055	0.746	0.076	0.017	0.001	4.020
PT.27	1.982	0.003	0.089	0.099	0.003	1.070	0.636	0.103	0.019	0.008	4.012

Experiment no.		Pressure	Temperature	Duration	*n*	SiO_2	TiO_2	Al_2O_3	Cr_2O_3	FeO total	MnO	MgO	NiO	CaO	Na_2O	Total
Opx	PT.22 R	3	1150	120	13	55.61	0.11	3.25	0.58	5.90	0.10	32.61	0.19	1.21	0.18	99.73
Opx	PT.1	3	1200	120	6	54.93	0.10	3.91	0.71	5.86	0.10	31.96	0.13	1.59	0.30	99.59
Opx	HPT.3	3	1200	120	12	54.77	0.01	3.11	0.54	8.66	0.13	30.68	0.03	1.42	0.32	99.66
Opx	CRPT.16	3	1250	120	11	54.25	0.10	4.33	1.18	5.77	0.09	31.55	0.33	1.73	0.23	99.57
Opx	PT.29 R	3.5	1150	120	11	56.11	0.12	2.30	0.55	5.62	0.11	33.36	0.23	1.16	0.20	99.75
Opx	HPT.4	3.5	1200	120	12	54.80	0.01	2.58	0.45	8.63	0.12	31.03	0.06	1.31	0.32	99.31
Opx	CRPT.22 R	3.5	1200	120	15	54.56	0.14	2.50	1.13	6.46	0.10	32.22	0.41	1.49	0.23	99.25
Opx	CRPT.21	3.5	1250	120	9	55.26	0.08	2.68	1.16	6.34	0.09	31.91	0.17	1.93	0.19	99.82
Opx	PT.37	3.5	1300	120	11	55.34	0.13	3.47	0.51	5.79	0.10	32.12	0.11	1.69	0.26	99.52
Opx	PT.47	3.5	1350	120	8	54.36	0.09	4.84	0.74	4.57	0.10	32.02	0.07	1.94	0.20	98.93
Opx	PT.35B R	3.5	1350	120	14	54.89	0.07	3.78	0.61	5.44	0.09	32.37	0.04	1.93	0.18	99.40
Opx	HPT.6	3.5	1400	120	12	53.80	0.01	4.52	0.66	7.74	0.12	29.74	0.01	2.06	0.35	99.00
Opx	PT.50	3.5	1400	120	10	54.47	0.09	4.08	0.65	4.90	0.09	32.13	0.03	2.16	0.24	98.82
Opx	PT.6	4	1100	120	4	55.89	0.10	1.74	0.41	5.30	0.08	34.46	0.25	0.99	0.10	99.31
Opx	PT.2	4	1200	120	2	56.03	0.08	2.25	0.42	6.07	0.09	33.17	0.25	1.39	0.26	100.03
Opx	CRPT.1	4	1200	120	14	55.77	0.13	1.76	0.80	5.53	0.10	33.91	0.27	1.30	0.21	99.77
Opx	CRPT.3 R	4	1200	120	14	55.34	0.13	2.08	1.04	6.28	0.09	31.88	0.41	1.93	0.25	99.44
Opx	PT.5	4	1300	120	2	55.38	0.05	3.22	0.61	4.53	0.09	33.33	0.02	2.01	0.20	99.42
Opx	PT.59	4	1300	120	18	56.52	0.10	2.92	0.51	5.46	0.10	32.46	0.24	2.19	0.26	100.77
Opx	PT.46	4	1350	120	8	55.06	0.08	3.46	0.59	5.35	0.10	32.01	0.06	2.16	0.24	99.11
Opx	CRPT.3	4	1350	120	14	55.47	0.14	2.91	1.19	4.95	0.11	32.60	0.08	2.03	0.28	99.76
Opx	PT.8	4	1400	120	9	55.64	0.08	3.39	0.54	6.20	0.09	32.36	0.14	2.13	0.23	100.79
Opx	PT.49	4	1400	120	15	55.57	0.06	3.67	0.58	4.51	0.08	32.46	0.03	2.22	0.23	99.41
Opx	PT.12	5	1200	168	9	58.33	0.07	1.31	0.30	4.74	0.07	35.28	0.22	1.17	0.18	101.66
Opx	PT.60	5	1250	120	7	56.38	0.06	1.49	0.28	5.78	0.08	33.92	0.12	1.34	0.10	99.54
Opx	PT.40 R	5	1300	120	7	56.23	0.06	1.44	0.39	6.56	0.08	33.35	0.24	1.77	0.19	100.31
Opx	PT.45	5	1400	168	10	56.58	0.07	2.10	0.38	6.22	0.09	32.74	0.05	1.90	0.23	100.37
Opx	PT.14	6	1200	168	13	56.35	0.06	0.78	0.22	4.64	0.07	35.31	0.16	0.88	0.13	98.60
Opx	PT.27	7	1200	12	9	57.65	0.06	0.72	0.32	4.28	0.08	33.97	0.29	1.49	0.28	99.14

Table 4 (continued)

Experiment no.	Si	Ti	Al	Fe^{2+}	Mn	Mg	Ca	Na	Cr	Ni	Total
PT.22 R	1.928	0.003	0.133	0.171	0.003	1.685	0.045	0.012	0.016	0.005	4.001
PT.1	1.911	0.002	0.160	0.170	0.003	1.657	0.059	0.020	0.019	0.004	4.007
HPT.3	1.926	Bdl	0.129	0.254	0.004	1.608	0.053	0.022	0.015	0.001	4.013
CRPT.16	1.893	0.003	0.178	0.168	0.003	1.641	0.065	0.016	0.032	0.009	4.007
PT.29 R	1.943	0.003	0.094	0.163	0.003	1.722	0.043	0.013	0.015	0.006	4.006
HPT.4	1.934	Bdl	0.107	0.255	0.004	1.632	0.050	0.022	0.013	0.002	4.017
CRPT.22 R	1.917	0.004	0.104	0.190	0.003	1.688	0.056	0.016	0.031	0.012	4.019
CRPT.21	1.927	0.002	0.110	0.185	0.003	1.659	0.072	0.013	0.032	0.005	4.007
PT.37	1.924	0.003	0.142	0.168	0.003	1.665	0.063	0.017	0.014	0.003	4.003
PT.47	1.893	0.002	0.199	0.133	0.003	1.663	0.072	0.014	0.020	0.002	4.002
PT.35B R	1.910	0.002	0.155	0.158	0.003	1.679	0.072	0.012	0.017	0.001	4.009
HPT.6	1.901	Bdl	0.188	0.229	0.004	1.566	0.078	0.024	0.018	bdl	4.008
PT.50	1.903	0.002	0.168	0.143	0.003	1.674	0.081	0.016	0.018	0.001	4.009
PT.6	1.941	0.003	0.071	0.154	0.002	1.785	0.037	0.007	0.011	0.007	4.018
PT.2	1.941	0.002	0.092	0.176	0.003	1.713	0.052	0.018	0.012	0.007	4.014
CRPT.1	1.936	0.003	0.072	0.160	0.003	1.754	0.049	0.014	0.022	0.008	4.021
CRPT.3 R	1.939	0.003	0.086	0.184	0.003	1.664	0.073	0.017	0.029	0.011	4.009
PT.5	1.919	0.001	0.131	0.131	0.003	1.722	0.075	0.013	0.017	0.001	4.012
PT.59	1.940	0.003	0.118	0.157	0.003	1.661	0.081	0.017	0.014	0.007	4.000
PT.46	1.922	0.002	0.142	0.156	0.003	1.666	0.081	0.016	0.016	0.002	4.005
CRPT.3	1.923	0.004	0.119	0.144	0.003	1.685	0.075	0.019	0.033	0.002	4.007
PT.8	1.917	0.002	0.138	0.179	0.003	1.662	0.079	0.015	0.015	0.004	4.013
PT.49	1.924	0.002	0.150	0.131	0.002	1.676	0.082	0.016	0.016	0.001	3.999
PT.12	1.970	0.002	0.052	0.134	0.002	1.776	0.042	0.011	0.008	0.006	4.004
PT.60	1.956	0.002	0.061	0.168	0.002	1.755	0.050	0.006	0.008	0.003	4.011
PT.40 R	1.949	0.002	0.059	0.190	0.002	1.723	0.066	0.013	0.011	0.007	4.021
PT.45	1.953	0.002	0.086	0.180	0.003	1.685	0.070	0.016	0.010	0.002	4.005
PT.14	1.963	0.002	0.032	0.135	0.002	1.834	0.033	0.009	0.006	0.005	4.020
PT.27	1.994	0.002	0.030	0.124	0.002	1.752	0.055	0.019	0.009	0.008	3.994

Cations calculated on the basis of 4 (olivine), 6 (pyroxene) or 12 (garnet) oxygens. All Fe as FeO.

bdl below detection limit of 0.01 wt%

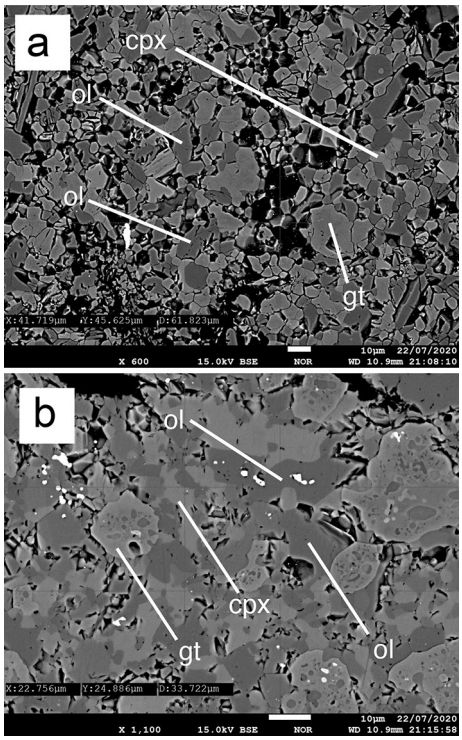

Fig. 1 BSE image of equilibrated experimental run products. (**a**) Experiment PT.60 (5 GPa, 1250 °C), (**b**) CRPT.22 R (3.5 GPa, 1250 °C)

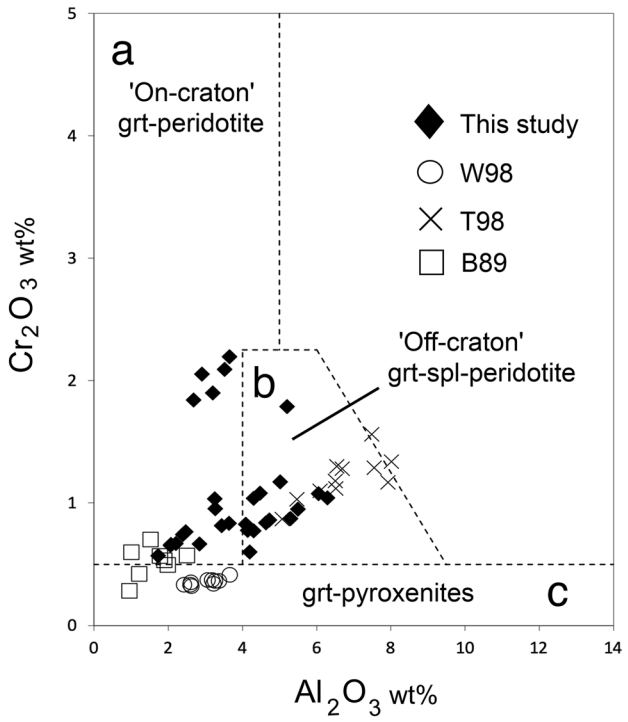

Fig. 2 Clinopyroxene Cr_2O_3 and Al_2O_3 wt% classification diagram of Ramsay (1992). Field a: Cratonic garnet-lherzolite. Field b: Non-cratonic garnet and garnet-spinel-lherzolite. Field c: Eclogite, pyroxenite source

Clinopyroxene

The size of cpx crystals ranged from < 10 to 30 µm. Compositional zoning and inclusions were not commonly observed in cpx, however, the well-equilibrated rims of the crystals were preferred for microanalysis. The concentration of Cr_2O_3 and Al_2O_3 wt% in cpx was consistent with the values expected for a natural cratonic garnet lherzolite and non-cratonic garnet-spinel lherzolite source, with values ranging from 0.57 to 2.0 wt% Cr_2O_3 and 1.7 to 6.3 wt% Al_2O_3 (Fig. 2). Na_2O in cpx ranged from 0.77 to 3.56 wt %. High Al_2O_3 cpx were produced from low-*P* high-*T* runs, and high Na_2O cpx from low-*P* low-*T* runs. The Cr# of cpx increased with increasing *P*, ranging from ca. 0.1−0.15 at 3 GPa to ca. 0.15−0.20 between 5 and 7 GPa. The CaO abundance in cpx was comparable to previously published analyses (e.g. Taylor 1998), and ranged from approximately 10 to 20 wt%, which is consistent with the concentrations expected for the PT range of our experiments. The Cr:Na ratio of cpx ranged from 0.11 to 0.76, with a mean value of 0.33.

Olivine

The size of experimental olivine crystals ranged from 15 to 40 µm. The Mg# (Mg/(Mg + Fe)) of olivine ranged from 0.84 to 0.96. Olivine grains did not display compositional zoning and crystals were typically free of inclusions.

Garnet

Garnet crystals ranged in size from 20 to > 40 µm. All microanalyses were performed on the well equilibrated rims of these crystals. Well equilibrated garnet displayed well-defined grain boundaries and had cation totals ≅ 8. Garnet synthesized from the Cr-MPY starting composition contained numerous Cr-spinel inclusions (Fig. 1b). The presence of spinel in Cr-enriched systems at high pressures is well known and has been discussed in considerable detail by Klemme (2004). The presence of Cr-rich spinel in these experiments is not expected to affect the solubility of Cr in cpx in equilibrium with garnet. These inclusions were typically < 5 µm and were not quantitatively analysed, and were avoided in the garnet analyses. The concentration of Ca and ΣFe in garnet decreased with increased *P* and *T*, and Mg increased with increased *P* and *T*. Cr_2O_3 contents in the experimental garnets ranged from 1.22 to 5.97 wt %, and the Cr# ranged from 0.03 to 0.17, which broadly covers the range observed in most natural lherzolitic garnets.

Orthopyroxene

Orthopyroxene produced from our experiments ranged in size from 10 to > 50 µm. Orthopyroxene crystals were unzoned and typically free of inclusions. The concentration of Al_2O_3 in orthopyroxene decreased with increasing *P*, ranging from 4.33 wt% at 3 GPa to 0.72 wt% at 7 GPa. The concentration of Cr_2O_3 also decreased with increasing *P* ranging from 1.17 wt% at 3 GPa to 0.31 wt% at 7 GPa. The concentration of SiO_2 and MgO in orthopyroxene increased with *P*, whereas CaO concentrations increased with increased *T*. The Mg# of our experimental orthopyroxene ranged from 0.86 to 0.95. The concentration of Na_2O ranged between 0.09 and 0.45 wt% and decreased marginally with increasing *P*. The highest Na_2O concentration in orthopyroxene were typically found in samples that equilibrated at low *P* (< 4 GPa).

Geobarometer calibration

The Cr-in-cpx geobarometer is based on the *P* dependent exchange of Cr between lherzolitic grt and cpx, expressed by Nimis and Taylor (2000) as:

$$\mathrm{CaMgSi_2O_6} + \mathrm{CaCrAlSiO_6} = \frac{1}{2}\left(\mathrm{Ca_2Mg}\right)\mathrm{Cr_2Si_3O_{12}} + \frac{1}{2}\left(\mathrm{Ca_2Mg}\right)\mathrm{Al_2Si_3O_{12}} \quad (1)$$

Or

$$\mathrm{di} + \mathrm{CaCrTs} = \frac{1}{2}\mathrm{uv_2kn_1} + \frac{1}{2}\mathrm{grs_2pyrp_1} \quad (2)$$

where diopside (di) and the CaCr Tschermak components in cpx (CaCrTs) react to give uvarovite (uv), knorringite (kn), grossular (grs), and pyrope (pyp) components in coexisting garnet. The corresponding equilibrium constant for this reaction is defined as:

$$\mathrm{K} = \frac{\left[a^{\mathrm{grt}}_{\mathrm{grs_2pyp_1}}\right]^{\frac{1}{2}} \cdot \left[a^{\mathrm{grt}}_{\mathrm{uv_2kn_1}}\right]^{\frac{1}{2}}}{\left[a^{\mathrm{cpx}}_{\mathrm{di}}\right] \cdot \left[a^{\mathrm{cpx}}_{\mathrm{CaCrTs}}\right]} \quad (3)$$

However, development of this geobarometer through an equilibrium constant requires thermodynamic data that is overcomplicated given the intended purpose of this geobarometer and, in some instances, are unavailable (see Nimis and Taylor, 2000 for discussion). As an alternative, we have continued to pursue this geobarometer in a similar manner to NT00 by using only the activity of the CaCrTs component of cpx. We have calculated $a^{\mathrm{cpx}}_{\mathrm{CaCrTs}}$ using the same formulation as the original NT00 calibration, which is defined as:

$$a^{\mathrm{cpx}}_{\mathrm{CaCrTs}} = \mathrm{Cr} - 0.81 \cdot \mathrm{Cr\#^{cpx}} \cdot (\mathrm{Na} + \mathrm{K}) \quad (4)$$

The basis on which $a^{\mathrm{cpx}}_{\mathrm{CaCrTs}}$ in cpx is estimated is explained in greater detail in Nimis and Taylor (2000). Multiple linear regressions of our experimental dataset, which includes experiments completed in this study (Table 2) and the previously published experiments of Taylor (1998), Walter (1998) and Brey et al. (1990) (Table 3), using *T*(K), $\mathrm{Cr\#^{cpx}}$, and $-T(\mathrm{K})\ln\left(a^{\mathrm{cpx}}_{\mathrm{CaCrTs}}\right)$ gave the following expression for *P* (Fig. 3):

$$P(\mathrm{GPa}) = 11.03 + \left(-T(\mathrm{K})\ln(a^{\mathrm{cpx}}_{\mathrm{CaCrTs}}) \times 0.001088\right) + \left(1.526 \times \ln\left(\frac{\mathrm{Cr\#^{cpx}}}{T(\mathrm{K})}\right)\right) \quad (5)$$

where $\mathrm{Cr\#^{cpx}} = \left(\frac{\mathrm{Cr}}{\mathrm{Cr+Al}}\right)$, $a^{\mathrm{cpx}}_{\mathrm{CaCrTs}} = \mathrm{Cr} - 0.81 \cdot \mathrm{Cr\#^{cpx}} \cdot (\mathrm{Na} + \mathrm{K})$, with all mineral components calculated assuming six oxygen anions per formula unit in clinopyroxene.

High *P* experiments from Walter (1998) and Brey et al. (1990) were used in our calibration to increase the number of data points at pressures above 5 GPa. Both experimental datasets used complex starting compositions similar to those listed in Table 1, which resulted in similar phase compositions to those reported in Table 4 at comparable PT conditions. The Walter (1998) experiments also provided a greatly extended *T* range, which widened the surface of the $\ln\left(\frac{\mathrm{Cr\#^{cpx}}}{T(\mathrm{K})}\right)$ axis in Fig. 3. Although the experiments of Walter (1998) were completed at near- solidus temperatures (see Table 3), these experiments provide an important constraint for cpx with low aCaCrTs. The inclusion of these experiments into our calibration improved the overall fit of our

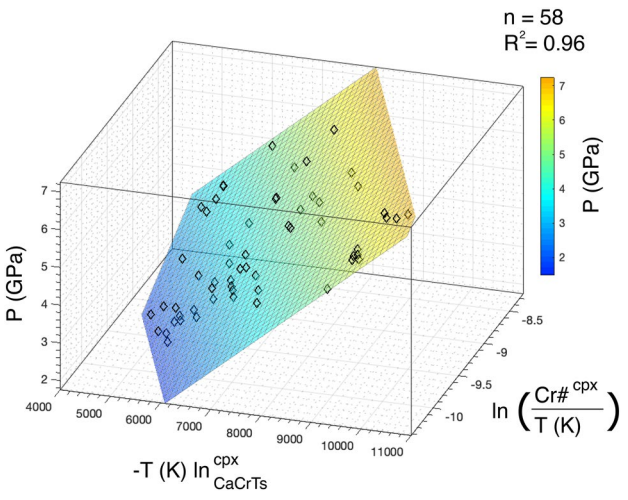

Fig. 3 Variation in −T(K), ln $(a^{\mathrm{cpx}}_{\mathrm{CaCrTs}})$ and ln $\left(\frac{\mathrm{Cr\#^{cpx}}}{T(\mathrm{K})}\right)$ plot against experimental *P* (kbar) using the experiments described in Tables 2 and 3

geobarometer regression equation to the experimental dataset. Thus the inclusion of these experiments in our dataset and calibration increases the R^2 of the geobarometer regression equation from approximately 0.93 to 0.963, with only a very slight change in estimated P (< 0.1 GPa) relative to that based solely on our new experiments when applied to natural cpx from Diavik. Some lower pressure experiments of Taylor (1998) were also incorporated into our experimental dataset to help strengthen the performance of our calibration at $P < 3$ GPa. These experiments were performed using an HPY-40 starting composition which produced cpx with similar compositions as those reported in Table 4. The temperatures for the Taylor (1998) experiments ranged between 1050 and 1250 °C. Similarly, including the Taylor (1998) experiments in our calibration increases the R^2 value from 0.94 to 0.96, again with only minimal differences in estimated P (< 0.1 GPa) relative to a calibration based solely on our new experiments when applied to natural cpx from Diavik. The improved statistics and extended compositional range covered justify the inclusion of these additional experimental data in our calibration dataset.

Propagation of uncertainties

The measured PT conditions of multi-anvil, belt and piston cylinder experiments, and the measured major and minor oxide concentrations by WDS are all subject to small but cumulative uncertainties. In addition, experimental P between 4 and 7 GPa are subject to a higher degree of uncertainty than experiments below 4 GPa. To accurately determine the error of the estimated P of our updated geobarometer we have propagated all analytical and experimental uncertainties. In Eq. (5), uncertainties exist in the Cr, Na, and Al abundances measured by WDS, and the experimentally determined P and T. As suggested by Ziberna et al. (2016), the influence of analytical uncertainties on the very minor K contents can safely be neglected. The experimental P of piston cylinder experiments conducted below 4 GPa is subject to an estimated uncertainty of approximately 3%. For experiments P between 4–6 GPa and above 6 GPa this estimated uncertainty increases to approximately 5 and 7.5%, respectively. The W–Re and Pt–Rh thermocouples used to measure experimental T are highly precise and have an uncertainty of ~ 1%. Using the conventional WDS EPMA analytical procedure described above, the maximum uncertainty in the measured concentrations of Cr_2O_3, Na_2O, and Al_2O_3 are 5.4, 2.2, and 4.1%, respectively. These uncertainty values were obtained by performing repeated measurements on an *ASTIMEX Mineralogy* Cr-diopside standard using the analytical conditions described in the methods section. The uncertainty in estimated P for our updated geobarometer calibration was determined by taking the square root of the sum of the squares of these errors (in percentage), which is defined by the following equation:

$$\delta P = \sqrt{(\delta P\text{exp})^2 + (\delta T\text{exp})^2 + (\delta \text{Cr})^2 + (\delta \text{Na})^2 + (\delta \text{Al})^2}$$

This approach results in uncertainty values of ± 0.31 GPa for P estimates below 4 GPa, ± 0.35 GPa between 4–6 GPa, and ± 0.41 GPa for P estimates above 6 GPa.

Compositional effects

We investigate compositional effects on the performance of our updated Cr-in-cpx geobarometer by comparing the difference of the experimental P and the calculated P for our updated geobarometer ($P_{exp} - P_{calc}$) against the concentration of various cations in cpx. We also compare the difference between the Brey and Köhler (1990) (BKN90) calculated P and the calculated P of our updated geobarometer ($P_{BKN90} - P_{calc}$) with the composition of natural cpx from xenoliths sampled by the Diavik-Ekati kimberlite pipes.

For our experimental database, the $P_{exp} - P_{calc}$ ranges between −0.68 and 0.93 GPa, with a mean difference of −0.017 GPa. The variation in $P_{exp} - P_{calc}$ does not show any major correlation with the changes in the abundances of major cations in cpx. This is contrast to the original NT00 calibration, which has a $P_{exp} - P_{calc}$ that ranges between −0.33 GPa at lower P and > −1 GPa (−1.76) at 7 GPa (Fig. 4 a, b). The NT00 calibration also shows strong systematic correlations between Al, Cr, and Na with $P_{exp} - P_{calc}$ (Fig. 4 d, f, h) in contrast to our revised calibration (Fig. 4 c, e, g). Additionally, the variation in $P_{exp} - P_{calc}$ for our updated calibration does not show any major systematic correlation with a^{cpx}_{CaCrTs} (Fig. 5a) whereas the original NT00 calibration exhibits a strong increase in $P_{exp} - P_{calc}$ with decreasing a^{cpx}_{CaCrTs} (Fig. 5b). The calculated pressures using the BKN90 Al-in-orthopyroxene geobarometer and our updated calibration ($P_{BKN90} - P_{calc)}$ for xenoliths from the Diavik-Ekati kimberlite pipes are generally in good agreement with a mean difference of −0.23 GPa and ranging between −3.1 and + 2.9 GPa in the worst-case examples. Two major trends are observed from the comparison of $P_{BKN90} - P_{calc}$ with the composition of cpx. Firstly, $P_{BKN90} - P_{calc}$ is typically high for cpx that are strongly enriched in Al (> 0.20 Al cations per six oxygen anions in clinopyroxene) (Fig. 6a). Similarly, departures from agreement between the two geobarometers are also observed for cpx with low Cr# (< 0.10) (Fig. 6b). These compositions typically correspond to high temperature, off-craton cpx derived from spinel-garnet bearing peridotites. Secondly, $P_{BKN90} - P_{calc}$ increases with increasing Na in cpx. For cpx with > 0.20 Na cations, the $P_{BKN90} - P_{calc}$ was typically > 1 GPa. One highly sodic cpx (> 0.35 Na cations) recorded a $P_{BKN90} - P_{calc}$ of 3 GPa (Fig. 6c). Highly

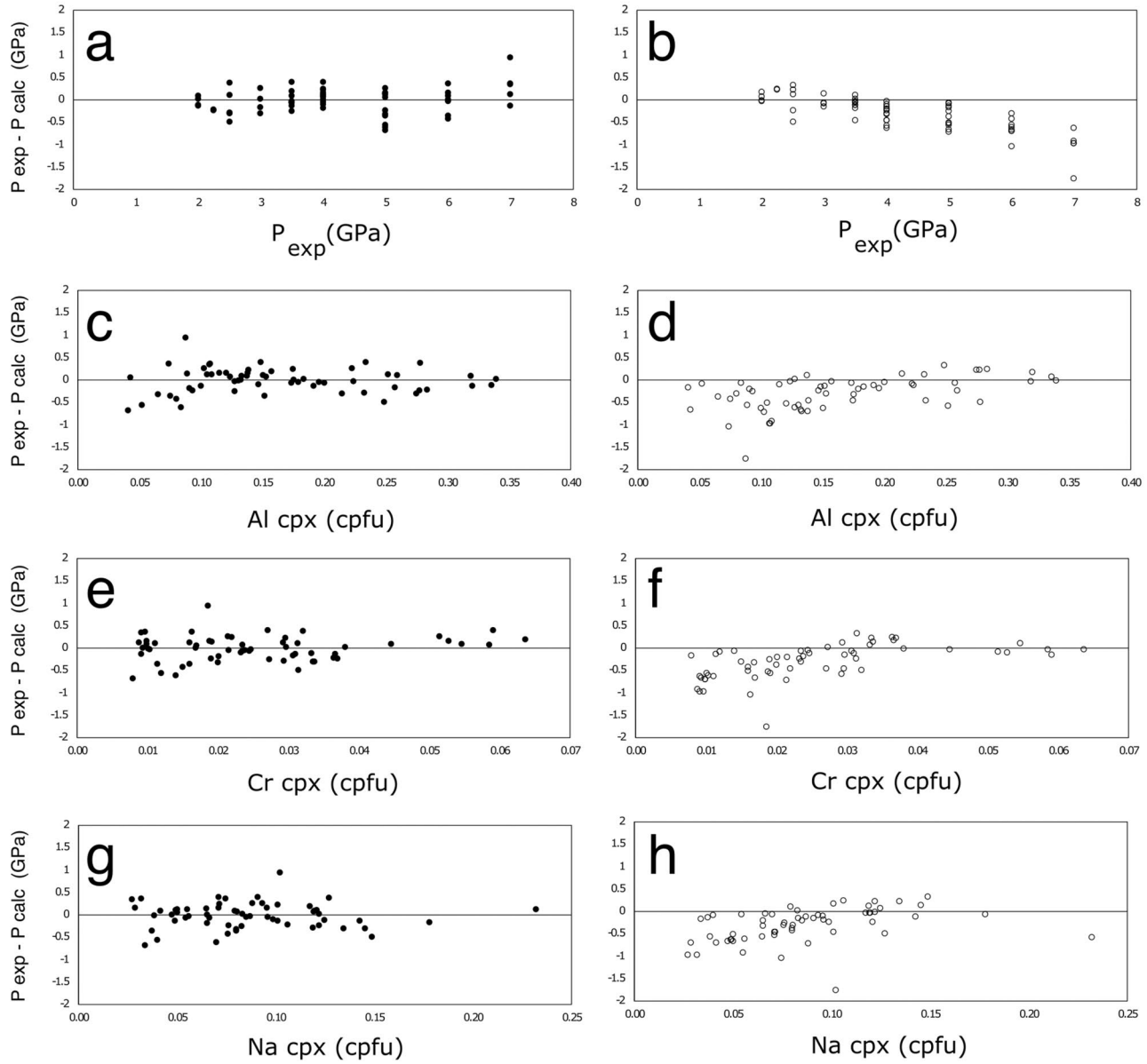

Fig. 4 Comparison between $P_{exp} - P_{calc}$ and the composition of cpx using our updated Cr-in-cpx geobarometer and the original NT00 geobarometer. Diagram is constructed using cpx from the experiments listed in Tables 2 and 3. P_{calc} is calculated P in GPa using either the updated geobarometer presented in this study (filled circles) or the original NT00 geobarometer (open circles) pressure for both geobarometers were made using the fixed experimental T

sodic cpx are commonly observed in eclogite xenoliths. The magnitude of $P_{BKN90} - P_{calc}$ is generally higher at very low levels of a^{cpx}_{CaCrTs} (Fig. 6d). This trend reflects the increase in uncertainty of P estimates at high P (> 6 GPa) and low a^{cpx}_{CaCrTs}. The relationship between $P_{BKN90} - P_{calc}$ with a^{cpx}_{CaCrTs} and $\left(\frac{a^{cpx}_{CaCrTs}}{Cr\#^{cpx}}\right)$ does not exhibit any systematic trends or systematic differences which may otherwise suggest a bias or error in the calibration (Fig. 6e).

We therefore recommend the following updated compositional filters when applying our updated Cr-in-cpx geobarometer to natural xenolith and xenocryst cpx:

- The Cr_2O_3–Al_2O_3 cpx source lithology discrimination diagram of Ramsay (1992) (Fig. 5 of Nimis and Taylor, 2000) should be used as a first pass filter for removing high alumina cpx which may have been derived from high-temperature, off-craton spinel bearing peridotites. We suggest that P estimates on cpx outside of fields a and b on Fig. 2 should be interpreted with caution. The

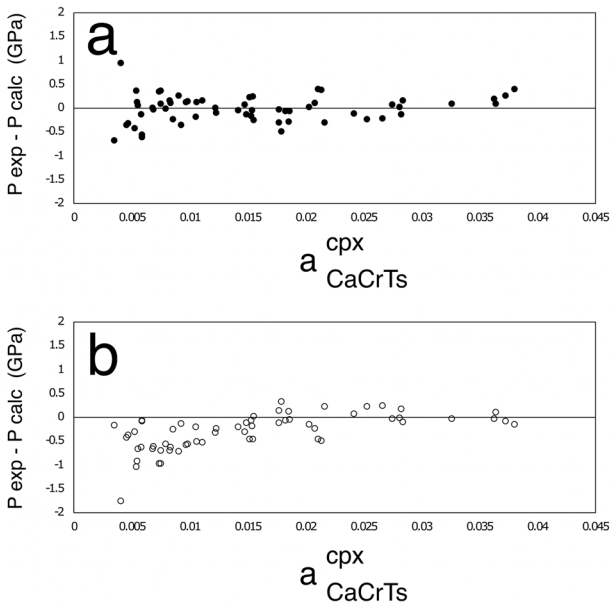

Fig. 5 Comparison between $P_{exp} - P_{calc}$ and the $\left(a^{cpx}_{CaCrTs}\right)$ of cpx using our updated Cr-in-cpx geobarometer and the original NT00 geobarometer. Diagram is constructed using cpx from the experiments listed in Tables 2 and 3. Symbols as Fig. 4

Cr_2O_3–Al_2O_3 relationship in cpx should also be used to test equilibrium with garnet. Cpx from the on-craton grt-peridotite field are preferred for single grain Cr-in-cpx geobarometry.

- *P* estimates on highly sodic cpx (> 0.20 Na cations) should be interpreted with caution regardless of Cr_2O_3 concentration in cpx. This filter should be used in conjunction with the Cr_2O_3–Al_2O_3 cpx source lithology discrimination diagram to determine whether a sodic cpx was derived from an eclogitic source. *P* estimates on eclogitic cpx should be discarded.
- The $Cr\#^{cpx}$ protocol of Ziberna et al. (2016) should be used to filter cpx with unsafe Cr# values, whereby $Cr\#^{cpx}$ outside of the range 0.10–0.65 should be discarded.
- We recommended the same data quality protocols as discussed above (see Ziberna et al. 2016), whereby cpx analyses with totals < 98 and > 102 wt%, and cation totals < 3.98 and > 4.02 (calculated on the basis of six oxygens in clinopyroxene) should be avoided.
- The a^{cpx}_{CaCrTs} range of the Cr-in-cpx geobarometer is extended to a lower concentration than suggested by NT00 and Ziberna et al. (2016). We recommend a lower limit of 0.005 for $\left(\frac{a^{cpx}_{CaCrTs}}{Cr\#^{cpx}}\right)$ in cpx, and analyses with below 0.005 should be discarded.

Comparison and applications

Garnet-lherzolite and garnet-pyroxenite xenoliths from the Diavik kimberlite pipe

An extensive database of analyses of cpx from garnet lherzolite and garnet pyroxenite xenoliths from the Diavik and Ekati kimberlite pipes within the Lac De Gras field in Canada's Northwest Territories (Aulbach et al. 2007; Creighton et al. 2010; Yaxley et al. 2017) has been used to test our updated Cr-in-cpx geobarometer. This database also includes a large dataset of cpx analyses sourced from heavy mineral concentrate (Supplementary File 1). A garnet peridotite/pyroxenite source for cpx from heavy mineral concentrate was confirmed through the use of the Cr_2O_3–Al_2O_3 cpx source lithology discrimination diagram of Ramsay (1992). PT estimates were calculated using the original NT00 calibration and our updated calibration of the Cr-in-cpx geobarometer in combination with the NT00 en-in-cpx geothermometer. For xenoliths, PT estimates were also determined using the BKN90 Al-in-orthopyroxene geobarometer and BKN90 two-pyroxene solvus geothermometer, and Nickel and Green (1985) Al-in-orthopyroxene geobarometer paired with the Taylor (1998) two-pyroxene solvus geothermometer. The *P* estimates for the various calibrations range from 3 to 7 GPa. The *P* estimates were broadly comparable below 4.5–5 GPa, however, the estimates on high *P* samples (≥ 4.5 GPa) showed an increasingly significant difference between the NT00 and our updated calibration of the Cr-in-cpx geobarometer (Table 5). The PT estimates for well-equilibrated xenoliths determined by our updated calibration were typically comparable to the Brey and Köhler (1990) estimates (Table 5). Xenoliths derived from *P* > 6.5 GPa provided a higher equilibration *P* when our updated calibration was applied. Similar observations were made for comparisons to the Nickel and Green (1985) and Taylor (1998) geothermobarometer (Table 5).

The PT estimates for the Diavik-Ekati xenoliths and xenocrysts using both the NT00 original and our revised Cr-in-cpx geobarometer [Eq. (5)] were used to construct paleogeotherms using the *FITPLOT* algorithm (Mather et al. 2011) (Fig. 7). Paleogeotherms were calculated assuming a 40 km crustal thickness (Davis et al. 2003; Snyder, 2008), and mantle isentrope of 1330 °C. The PT estimates using our modified calibration constitute a steep paleogeotherm that intersects the mantle isentrope approximately between 235 and 250 km (Fig. 7a). The estimates using the NT00 calibration form a shallower paleogeotherm that intersects the isentrope at the slightly shallower depth of approximately 210–220 km (Fig. 7b). The estimated depth to the lithosphere-asthenosphere boundary (LAB) using our updated calibration is comparable to LAB estimates of ~ 190−250 km

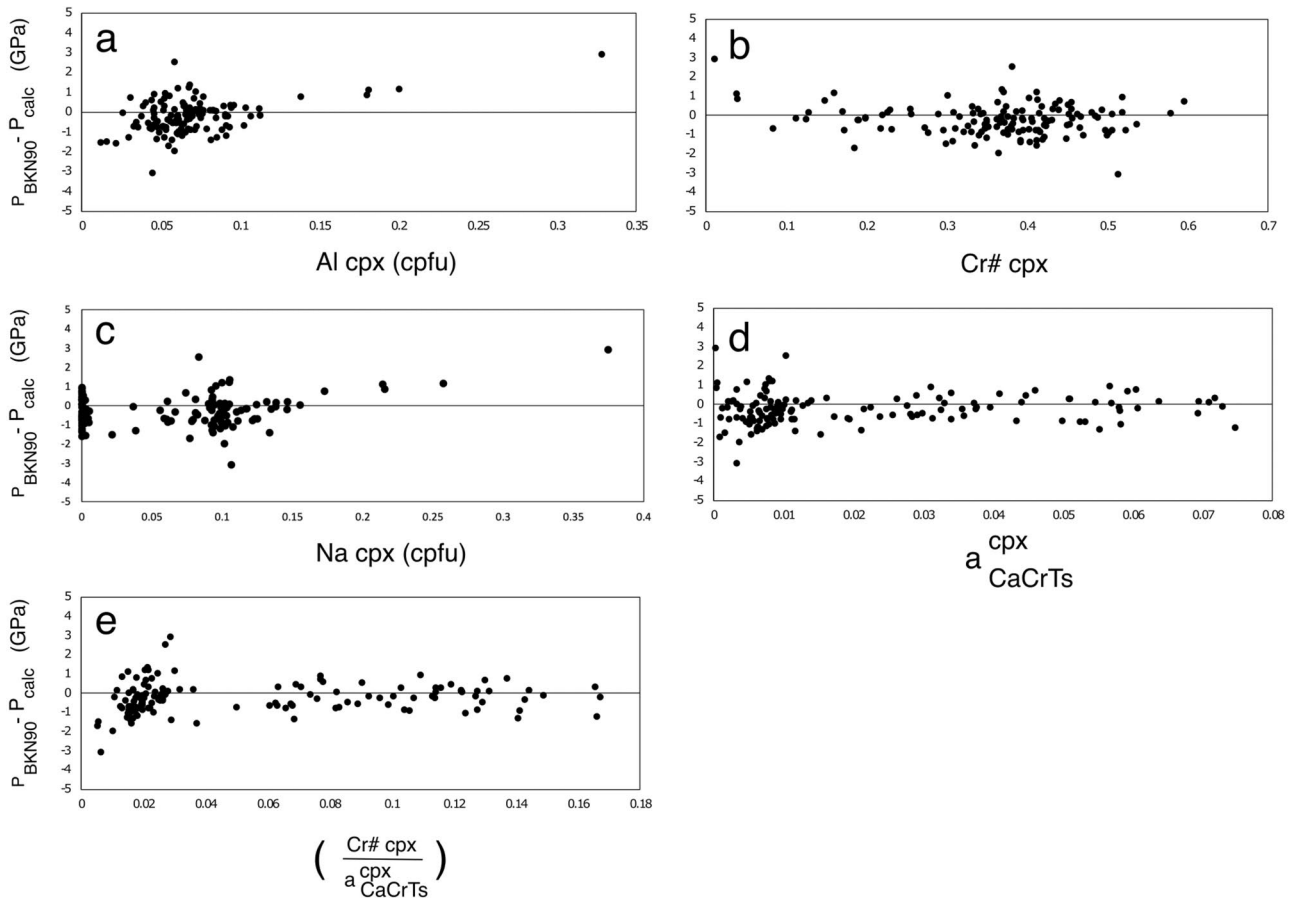

Fig. 6 Comparison between $P_{BKN90} - P_{calc}$ and the composition of cpx using our updated Cr-in-cpx geobarometer and the original NT00 geobarometer. Diagram is constructed using cpx and xenolith data from the Diavik-Ekati kimberlite pipes. BKN90 is Brey and Köhler (1990) Al-in-orthopyroxene equilibration *P*, calculated using the *T* estimates of the Brey and Kohler two-pyroxene solvus geothermometer. See Comparison and application for Diavik-Ekati sample references

Table 5 Comparison of estimated PT conditions (in GPa, °C) for selected equilibrated mantle xenoliths from various kimberlite pipes

Location	Sample no.	References	*P* this study *T* NT00	*P* NT00 *T* NT00	*P* BKN90 *T* BKN90	*P* NG85 *T* TA98
Diavik	DDM360	Mather (2012)	7.0–1262	6.0–1238	7.0–1297	6.5–1265
Diavik	DDM327	Mather (2012)	7.8–1323	6.6–1294	7.9–1365	7.1–1325
Diavik	MX131	Creighton et al. (2010)	6.2–1237	5.4–1221	6.3–1280	5.9–1244
Diavik	YKL915	Aulbach et al. (2007)	4.7–760	3.5–738	4.5–824	4.0–768
Diavik	VR50914	Aulbach et al. (2007)	3.0–748	2.6–743	3.3–795	3.3–770
Diavik	YK2474	Aulbach et al. (2007)	5.2–1055	4.7–1048	5.1–1121	5.1–1068

for the central Slave Craton derived previously from geothermobarometry on mantle xenoliths and xenocrysts (Griffin et al. 1999, 2004; Aulbach et al., 2018) and from various geophysical techniques, including magneto-telluric (MT) methods (Jones et al., 2003), seismic tomography (Bank et al. 2000), and through strain rate measurements (Eaton et al. 2009).

Cr diopside xenoliths and xenocrysts from the Argyle lamproite pipe

Equilibration PT conditions were also calculated for a suite of Cr-diopside xenocrysts from heavy mineral concentrate (Jaques et al. 2018) and mantle peridotite xenoliths (Luguet et al. 2009) from the Argyle lamproite pipe in Western Australia. This provides a practical example of the usefulness

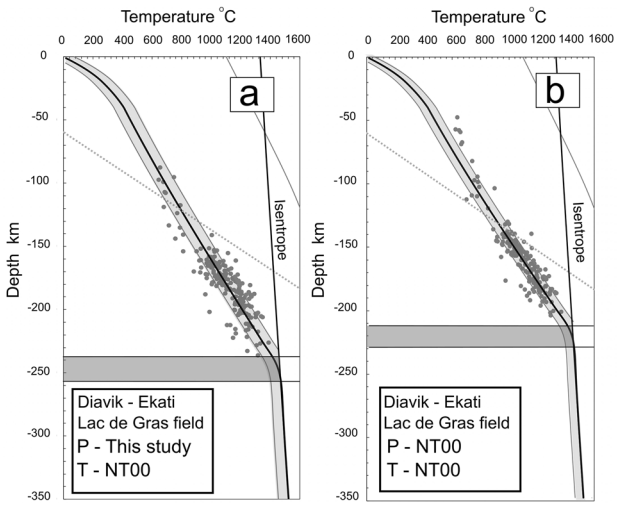

Fig. 7 Paleogeothermal gradients for the Lac De Gras (Diavik-Ekati) kimberlite field (Canada). The paleogeotherms were constructed using *FITPLOT* (Mather et al. 2011) using PT data derived from (**a**) our revised Cr-in-cpx geobarometer [Eq. (5)], and (**b**) the original Nimis and Taylor (2000) calibration. *T* for both geobarometers were calculated using the NT00 en-in-cpx single crystal geothermometer, with the final PT estimate solved by iteration. See text and Supplementary File 1 xenocryst data. See text for *FITPLOT* input parameters and sample references. Shaded margin is the *FITPLOT* error only. Graphite-diamond transition from Kennedy and Kennedy (1976)

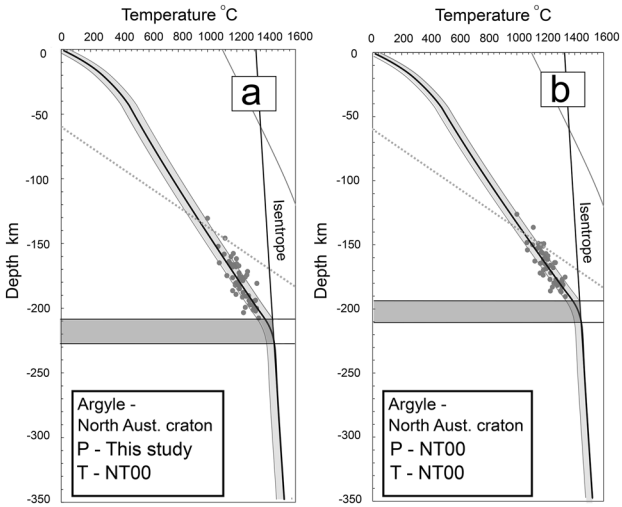

Fig. 8 Paleogeothermal gradients for the Argyle lamproite (Australia). The paleogeotherms were constructed using *FITPLOT* (Mather et al. 2011) using PT data derived from (**a**) our revised Cr-in-cpx geobarometer [Eq. (5)], and (**b**) the original Nimis and Taylor (2000) calibration. *T* for both geobarometers were calculated using the NT00 en-in-cpx single crystal geothermometer, with the final PT estimate solved by iteration. See text for xenocryst references. See text for *FITPLOT* input parameters. Shaded margin is the *FITPLOT* error only. Graphite-diamond transition from Kennedy and Kennedy (1976)

of single-crystal geothermobarometry as the garnet in the Argyle mantle peridotites is typically retrogressed and altered (Jaques et al. 1990). A *FITPLOT* paleogeotherm was calculated for a crustal thickness of 42 km crustal thickness (Kennett et al. 2011) and other parameters as above using our revised Cr-in-cpx geobarometer and the original NT00 geobarometer (Fig. 8). The *FITPLOT* paleogeotherm based on our Cr-in-cpx calibration is steeper than that generated from the NT00 calibration and results in an estimated LAB 210−215 km compared with 200 km for the NT00 calibration (Fig. 8). The estimated LAB depth at 210−215 km compares well with *s* wave seismic tomography models which indicate a present-day lithospheric thickness of ~ 200−250 km (Fishwick and Rawlinson, 2012; Hoggard et al. 2020).

Conclusions

An updated high-*P* experimental dataset that includes mineral data from new experiments conducted between 3–7 GPa and 1050–1400 °C, and published data from Brey et al. (1990), Taylor (1998) and Walter (1998) has been used to re-examine the solubility of Cr in cpx in garnet-bearing lherzolites. Statistical treatment of this dataset has derived an alternative calibration for the widely used Nimis and Taylor (2000) Cr-in-cpx geobarometer. Our modified calibration addresses the progressive and systematic underestimation of *P* above 4 GPa by the original NT00 Cr-in-Cpx geobarometer calibration. The empirical recalibration of NT00 geobarometer proposed by Nimis et al. (2020) appears to provide a closer approximation for pressures in the 4.5–6 GPa interval but still carries significant uncertainties at higher pressure due to the small number of xenoliths equilibrated at and above 6 GPa. The improved reliability and precision of our calibration for *P* estimates > 5 GPa has been demonstrated through application to cpx from garnet-lherzolite and garnet-pyroxenite xenoliths from the Diavik-Ekati kimberlite and Argyle lamproite pipes. The estimated paleogeotherms constructed using our new PT estimates differ slightly from previous estimates based on the NT00 geobarometer, resulting in a modest but significant increase in the estimated lithospheric thickness beneath these kimberlites and lamproite. Our updated paleogeotherms for Diavik-Ekati and Argyle are in line with estimates from seismic tomography and MT surveys. Application of the new calibration of the Cr-in-cpx geobarometer can be expected to result in higher *P* estimates for Cr-diopside xenoliths and xenocrysts derived from garnet-lherzolites equilibrated at pressures beyond 5 GPa relative to the NT00 version. These estimates will lead to deeper estimates of the depth to the LAB beneath many cratons, which will allow the nature of the cratonic lithosphere to be more accurately studied in future investigations.

Acknowledgements All EPMA Analyses were completed at the Centre for Advanced Microscopy an advanced imaging precinct of Microscopy Australia, a facility that is funded by the Australian National University, and State and Federal Governments. Jeff Chen is thanked for his assistance with the EPMA analyses. ZS was the recipient of an Australian Government funded domestic student RTP PhD scholarship and stipend. We thank Karol Czarnota of Geoscience Australia for his interest and support of this project. We thank Graham Pearson for providing access to the *FITPLOT* program. Paolo Nimis and Vincenzo Stagno are kindly thanked for their constructive reviews, which greatly improved the overall clarity of the manuscript, and also Daniela Rubatto for editorial handling.

References

Aulbach S, Pearson NJ, O'reilly SY, Doyle BJ (2007) Origins of xenolithic eclogites and pyroxenites from the central slave craton. Can J Petrol 48(10):1843–1873

Aulbach S, Heaman LM, Stachel T (2018) The diamondiferous mantle root beneath the central slave craton. In: Davy T et al (eds) Geoscience and exploration of the Argyle, Bunder, Diavik, and Murowa diamond deposits Special publication 20. Society of Economic Geologists, Littleton, pp 319–339

Bank C, Bostock M, Ellis R, Cassidy J (2000) A reconnaissance teleseismic study of the upper mantle and transition zone beneath the Archean slave craton in NW Canada. Tectonophysics 319(3):151–166

Bose K, Ganguly J (1995) Quartz-coesite transition revisited: reversed experimental determination at 500–1200 C and retrieved thermochemical properties. Am Miner 80(3–4):231–238

Brey G, Köhler T (1990) Geothermobarometry in four-phase lherzolites II. New thermobarometers, and practical assessment of existing thermobarometers. J Petrol 31(6):1353–1378

Brey G, Köhler T, Nickel K (1990) Geothermobarometry in four-phase lherzolites I. Experimental results from 10 to 60 kb. J Petrol 31(6):1313–1352

Carswell D (1991) The garnet-orthopyroxene Al barometer: problematic application to natural garnet lherzolite assemblages. Miner Mag 55(378):19–31

Cookenboo H, Grütter H (2010) Mantle-derived indicator mineral compositions as applied to diamond exploration. Geochem Explor Environ Anal 10(1):81–95

Creighton S, Stachel T, Eichenberg D, Luth RW (2010) Oxidation state of the lithospheric mantle beneath Diavik diamond mine, central slave craton, NWT. Can Contrib Miner Petrol 159(5):645–657

Davis W, Jones A, Bleeker W, Grütter H (2003) Lithosphere development in the slave craton: a linked crustal and mantle perspective. Lithos 71(2–4):575–589

Eaton DW, Darbyshire F, Evans RL, Grütter H, Jones AG, Yuan X (2009) The elusive lithosphere–asthenosphere boundary (LAB) beneath cratons. Lithos 109(1–2):1–22

Fishwick S, Rawlinson N (2012) 3-D structure of the Australian lithosphere from evolving seismic datasets. Aust J Earth Sci 59:809–826

Green DH (2015) Experimental petrology of peridotites, including effects of water and carbon on melting in the earth's upper mantle. Phys Chem Miner 42(2):95–122

Green DH, Falloon TJ (1998) Pyrolite: a ringwood concept and its current expression. The earth's mantle composition, structure, and evolution. Cambridge University Press, Cambridge, pp 311–380

Griffin W, Doyle B, Ryan C, Pearson N, Suzanne YOR, Davies R, Kivi K, Van Achterbergh E, Natapov L (1999) Layered mantle lithosphere in the Lac de Gras area, slave craton: composition, structure and origin. J Petrol 40(5):705–727

Griffin W, O'Reilly SY, Doyle B, Pearson N, Coopersmith H, Kivi K, Malkovets V, Pokhilenko N (2004) Lithosphere mapping beneath the North American plate. Lithos 77(1–4):873–922

Grütter HS, Gurney JJ, Menzies AH, Winter F (2004) An updated classification scheme for mantle-derived garnet, for use by diamond explorers. Lithos 77(1–4):841–857

Gung Y, Panning M, Romanowicz B (2003) Global anisotropy and the thickness of continents. Nature 422(6933):707–711

Hoggard MJ, Czarnota K, Richards FD, Huston DL, Jaques AL, Ghelichkhan S (2020) Global distribution of sediment-hosted metals controlled by craton edge stability. Nat Geosci 13:504–510

Jaques AL, O'Neill HSC, Smith CB, Moon J, Chappell BW (1990) Diamondiferous peridotite xenoliths from the Argyle (AK1) lamproite pipe, Western Australia. Contrib Miner Petrol 104:255–276

Jaques AL, Luguet A, Smith CB, Pearson D, Yaxley GM, Kobussen A (2018) Nature of the mantle beneath the Argyle AK1 lamproite pipe: constraints from mantle xenoliths, diamonds, and lamproite geochemistry. In: Davy T et al (eds) Geoscience and exploration of the Argyle, Bunder, Diavik, and Murowa diamond deposits Special publication 20. Society of Economic Geologists, Littleton, pp 119–143

Jones AG, Lezaeta P, Ferguson IJ, Chave AD, Evans RL, Garcia X, Spratt J (2003) The electrical structure of the slave craton. Lithos 71(2–4):505–527

Kennedy CS, Kennedy GC (1976) The equilibrium boundary between graphite and diamond. J Geophys Res 81(14):2467–2470

Kennett BLN, Salmon M, Saygin E, AW Group (2011) AusMoho: the variation of Moho depth in Australia. Geophys J Int 187:946–958

Klemme S (2004) The influence of Cr on the garnet–spinel transition in the earth's mantle: experiments in the system MgO–Cr_2O_3–SiO_2 and thermodynamic modelling. Lithos 77(1–4):639–646

Lee C-TA, Lenardic A, Cooper CM, Niu F, Levander A (2005) The role of chemical boundary layers in regulating the thickness of continental and oceanic thermal boundary layers. Earth Planet Sci Lett 230(3–4):379–395

Leinenweber KD, Tyburczy JA, Sharp TG, Soignard E, Diedrich T, Petuskey WB, Wang Y, Mosenfelder JL (2012) Cell assemblies for reproducible multi-anvil experiments (the COMPRES assemblies). Am Miner 97(2–3):353–368

Luguet A, Jaques AL, Pearson DG, Smith CB, Bulanova GP, Roffey SL, Rayner J, Lorand J-P (2009) An integrated petrological, geochemical and Re–Os isotope study of peridotite xenoliths from the Argyle lamproite, Western Australia and implications for cratonic diamond occurrences. Lithos 112(2):1096–1108

Mather K (2012) A xenolith-based lithospheric transect of the slave craton. PhD Thesis, Durham University, Durham, NWT, Canada

Mather KA, Pearson DG, McKenzie D, Kjarsgaard BA, Priestley K (2011) Constraints on the depth and thermal history of cratonic lithosphere from peridotite xenoliths, xenocrysts and seismology. Lithos 125(1–2):729–742

Nickel K (1986) Phase equilibria in the system SiO_2–MgO–Al_2O_3–CaO–Cr_2O_3 (SMACCR) and their bearing on spinel/garnet lherzolite relationships. Neues Jahrb Miner Abh 155:259–287

Nickel K, Green D (1985) Empirical geothermobarometry for garnet peridotites and implications for the nature of the lithosphere, kimberlites and diamonds. Earth Planet Sci Lett 73(1):158–170

Nimis P, Taylor WR (2000) Single clinopyroxene thermobarometry for garnet peridotites. Part I. Calibration and testing of a Cr-in-Cpx barometer and an enstatite-in-Cpx thermometer. Contrib Miner Petrol 139(5):541–554

Nimis P, Preston R, Perritt SH, Chinn IL (2020) Diamond's depth distribution systematics. Lithos 376:105729

Pouchou J-L, Pichoir F (1991) Quantitative analysis of homogeneous or stratified microvolumes applying the model "PAP." Electron probe quantitation. Springer, New York, pp 31–75

Ramsay RR (1992) Geochemistry of diamond indicator minerals. PhD Thesis, University of Western Australia

Shirey SB, Cartigny P, Frost DJ, Keshav S, Nestola F, Nimis P, Pearson DG, Sobolev NV, Walter MJ (2013) Diamonds and the geology of mantle carbon. Rev Mineral Geochem 75(1):355–421

Snyder DB (2008) Stacked uppermost mantle layers within the Slave craton of NW Canada as defined by anisotropic seismic discontinuities. Tectonics. https://doi.org/10.1029/2007TC002132

Taylor W (1998) An experimental test of some geothermometer and geobarometer formulations for upper mantle peridotites with application to the thermobarometry of fertile lherzolite and garnet websterite. Neues Jahrb Mineral Abhandlungen 172:381–408

Walter MJ (1998) Melting of garnet peridotite and the origin of komatiite and depleted lithosphere. J Petrol 39(1):29–60

Yaxley GM, Green DH (1998) Reactions between eclogite and peridotite: mantle refertilisation by subduction of oceanic crust. Schweiz Mineral Petrogr Mitt 78(2):243–255

Yaxley GM, Berry A, Rosenthal A, Woodland A, Paterson D (2017) Redox preconditioning deep cratonic lithosphere for kimberlite genesis–evidence from the central slave craton. Sci Rep 7(1):1–10

Ziberna L, Nimis P, Kuzmin D, Malkovets VG (2016) Error sources in single-clinopyroxene thermobarometry and a mantle geotherm for the Novinka kimberlite. Yakutia Am Mineral 101(10):2222–2232

Authors and Affiliations

Z. J. Sudholz[1] · G. M. Yaxley[1] · A. L. Jaques[1] · G. P. Brey[2]

[1] Research School of Earth Sciences, Australian National University, Canberra, ACT 2601, Australia

[2] Institut Für Geowissenschaften, Goethe Universität, 60438 Frankfurt am Main, Germany